Bifurcation analysis and computer simulation of biaxial liquid crystals

Giovanni De Matteis,[1,2,*] Silvano Romano,[3,†] and Epifanio G. Virga[2,‡]
[1]*Scuola Normale Superiore di Pisa, Piazza dei Cavalieri 7, I-56126 Pisa, Italy*
[2]*Dipartimento di Matematica, Istituto Nazionale per la Fisica della Materia, Università di Pavia, via Ferrata 1, I-27100 Pavia, Italy*
[3]*Istituto Nazionale per la Fisica della Materia and Dipartimento di Fisica "A. Volta," Università di Pavia, via A. Bassi 6, I-27100 Pavia, Italy*
(Received 29 January 2005; revised manuscript received 19 July 2005; published 12 October 2005)

We extend the analysis of a mean-field model for biaxial liquid crystals recently proposed by Sonnet *et al.* [Phys. Rev. E **67**, 061701 (2003)]. In particular, we perform a bifurcation analysis of the equilibrium equations and derive the complete phase diagram. We show that two order parameters suffice to label all equilibrium phases, though they exhibit different bifurcation patterns. A Monte Carlo simulation study is performed as well, confirming qualitatively the predictions of this analysis.

DOI: 10.1103/PhysRevE.72.041706 PACS number(s): 61.30.Cz, 61.30.Dk

I. INTRODUCTION

In the last few years great interest has been paid to biaxial nematic liquid crystals, both experimentally and theoretically [1]. Stable biaxial phases have been observed in lyotropic systems as early as 1980 [2]. Since 1986 there have been a number of reports of thermotropic biaxiality in low-molecular weight compounds [3–6]. Recently, Madsen *et al.* [7] and Acharya *et al.* [8,9] reported the detection of a biaxial nematic phase in thermotropic liquid crystals composed of bow-shaped molecules. Moreover, biaxiality has also been discovered in polymeric systems [10].

More recently, Merkel *et al.* [11] observed experimental evidence of biaxiality in two different mesogenic molecular *tetrapodes*. These molecules, which exhibit biaxiality close to room temperature, provided the first quantitative observation for this class of liquid crystals. In an individual tetrapode, four rodlike molecules are connected to a siloxane core through four siloxane spacers, leading to a macromolecule having a platelet shape. This structure hampers the rotation of each rodlike constituent around its long axis, thus promoting biaxiality of the resulting phase.

Over the past 30 years, the possible effect of molecular biaxiality on nematic order has been studied theoretically. Molecular field models [12–23] and, later, simulation studies of lattice models [24–28], have shown that single-component models consisting of molecules possessing D_{2h} symmetry (platelets), and interacting by appropriately chosen potentials, can produce biaxial phases. A similar scenario has emerged from the analytical study of systems of biaxial molecules interacting via hard-core potentials [29], supported by simulation results [30]. In these works a second-order uniaxial-to-biaxial phase transition is found and a mostly singular direct isotropic-to-biaxial transition is predicted as well. However, a different scenario arises in Ref. [23], where the authors consider a particular model within the general expression of Straley's pair potential [15] and predict a range of parameters where a direct first-order transition occurs between biaxial and isotropic phases. Moreover, they predict biaxial-to-uniaxial transitions of both second- and first order, thus finding a tricritical point in the phase diagram. These results have also been confirmed by Monte Carlo studies [31]. The experimental findings of Merkel *et al.* [11] were interpreted within this theoretical setting and confirmed the existence of a tricritical point.

Here, we further pursue the study of the model proposed in Ref. [23] and confirm the existence of yet another tricritical point, now on the isotropic-to-biaxial transition line, already predicted in Ref. [32].

This paper is organized as follows. In Sec. II, we present the pair potential. In Secs. III and IV we perform a complete bifurcation analysis of the mean-field equations. Finally, in Sec. V we support the mean-field predictions with a Monte Carlo simulation. The main outcomes of the paper and the further questions it poses are summarized in Sec. VI.

II. INTERMOLECULAR POTENTIAL

In a recent work [23], a biaxial mesogenic interaction model has been proposed. It elaborates on Straley's general intermolecular potential, written in the form

$$V = -U_0\{\mathbf{q}\cdot\mathbf{q}' + \gamma(\mathbf{q}\cdot\mathbf{b}' + \mathbf{q}'\cdot\mathbf{b}) + \lambda(\mathbf{b}\cdot\mathbf{b}')\}, \qquad (1)$$

where the pairs of tensors $(\mathbf{q},\mathbf{b})$ and $(\mathbf{q}',\mathbf{b}')$ represent the interacting molecules. The tensor $\mathbf{q}$ is purely uniaxial around the unit vector $\boldsymbol{m}$ in the direction of the long molecular axis, while $\mathbf{b}$, orthogonal to $\mathbf{q}$, is purely biaxial

$$\mathbf{q} := \boldsymbol{m}\otimes\boldsymbol{m} - \frac{1}{3}\mathbf{I},$$

$$\mathbf{b} := \boldsymbol{e}\otimes\boldsymbol{e} - \boldsymbol{e}_\perp\otimes\boldsymbol{e}_\perp. \qquad (2)$$

Here, the orthonormal basis $\{\boldsymbol{e},\boldsymbol{e}_\perp,\boldsymbol{m}\}$ is the eigenframe of any molecular polarizability tensor, and so $\mathbf{q}$ and $\mathbf{b}$ represent the irreducible components of the anisotropic part of any such tensor.

*Electronic address: g.dematteis@sns.it
†Electronic address: romano@pv.infn.it
‡Electronic address: virga@imati.cnr.it

A generalization of Eq. (1) can be written as

$$V = \{\tilde{\xi}(\mathbf{q}\cdot\mathbf{q}') + \tilde{\gamma}(\mathbf{q}\cdot\mathbf{b}' + \mathbf{q}'\cdot\mathbf{b}) + \tilde{\lambda}(\mathbf{b}\cdot\mathbf{b}')\}. \quad (3)$$

Let $U_0 := \max(|\tilde{\xi}|, |\tilde{\gamma}|, |\tilde{\lambda}|)$. Upon scaling the parameters $\tilde{\xi}$, $\tilde{\gamma}$, and $\tilde{\lambda}$ to U_0, Eq. (3) becomes

$$V = -U_0\{\xi(\mathbf{q}\cdot\mathbf{q}') + \gamma(\mathbf{q}\cdot\mathbf{b}' + \mathbf{q}'\cdot\mathbf{b}) + \lambda(\mathbf{b}\cdot\mathbf{b}')\}, \quad (4)$$

where ξ, γ, λ are not greater than 1 in magnitude, and at least one of them equals 1 in magnitude; the case in Eq. (1) is recovered by choosing $\xi=1$.

It can easily be checked that, apart from an additional constant, the potentials in Eqs. (1) and (3) can also be given as symmetrized linear combinations involving squares of the nine different inner products between the vectors of the orthonormal basis $\{\boldsymbol{e},\boldsymbol{e}_\perp,\boldsymbol{m}\}$ and its analog $\{\boldsymbol{e}',\boldsymbol{e}'_\perp,\boldsymbol{m}'\}$. With the aid of some elementary geometric identities, it can actually be shown that any symmetrized linear combination of the named squared inner products reduces to a "diagonal" form, only involving the three squared inner products between corresponding unit vectors [31]; in formulas

$$V = -U_0\left\{-\left(\lambda+\frac{\xi}{3}\right) + (\xi-\lambda)(\boldsymbol{m}\cdot\boldsymbol{m}')^2 + 2(\lambda+\gamma)(\boldsymbol{e}'_\perp\cdot\boldsymbol{e}_\perp)^2 + 2(\lambda-\gamma)(\boldsymbol{e}'\cdot\boldsymbol{e})^2\right\}, \quad (5)$$

or, equivalently

$$V = \epsilon\{-\xi P_2(\boldsymbol{m}\cdot\boldsymbol{m}') + 2\gamma[P_2(\boldsymbol{e}'\cdot\boldsymbol{e}) - P_2(\boldsymbol{e}'_\perp\cdot\boldsymbol{e}_\perp)] - \lambda[2P_2(\boldsymbol{e}'_\perp\cdot\boldsymbol{e}_\perp) + 2P_2(\boldsymbol{e}'\cdot\boldsymbol{e}) - P_2(\boldsymbol{m}\cdot\boldsymbol{m}')]\}, \quad (6)$$

where $\epsilon := \frac{2}{3}U_0$ and $P_2(x) := \frac{1}{2}(3x^2-1)$ is the second Legendre polynomial.

Moreover, we are considering here molecules possessing D_{2h} symmetry: there are three mutually orthogonal mirror planes inducing inversion symmetry through their intersection. The expression in Eq. (5) clearly reflects the invariance of the intermolecular potential under this group. As a consequence, V can be written as a linear combination of symmetry-adapted functions $\{s_k(\hat{\omega})\}_{k=1,\ldots,4}$ (see, e.g., Refs. [26,27,29,31]) in the notation of Ref. [31], where $\hat{\omega}=(\hat{\varphi},\hat{\vartheta},\hat{\psi})$ denotes the triplet of Euler angles [33–35] defining the orientation of one molecule relative to the other

$$V(\hat{\omega}) = -\epsilon\{\xi s_1(\hat{\omega}) + \sqrt{6}\gamma[s_2(\hat{\omega}) + s_3(\hat{\omega})] + 6\lambda s_4(\hat{\omega})\}, \quad (7)$$

where

$$s_1(\hat{\omega}) = P_2(\cos\hat{\vartheta}),$$

$$s_2(\hat{\omega}) = \frac{\sqrt{6}}{4}\sin^2\hat{\vartheta}\cos 2\hat{\varphi},$$

$$s_3(\hat{\omega}) = \frac{\sqrt{6}}{4}\sin^2\hat{\vartheta}\cos 2\hat{\psi},$$

$$s_4(\hat{\omega}) = \frac{1}{4}(1+\cos^2\hat{\vartheta})\cos 2\hat{\varphi}\cos 2\hat{\psi} - \frac{1}{2}\cos\hat{\vartheta}\sin 2\hat{\varphi}\sin 2\hat{\psi}. \quad (8)$$

The notation in Eq. (6) has the advantage of easing comparison with the well-known and extensively studied Lebwohl-Lasher or Maier-Saupe P_2 potential, to which it reduces when $\gamma=\lambda=0$. Thus, the parameters λ and γ introduce different perturbations to this model. Simulation results suggest that the condition $\lambda=0$, $\gamma\neq 0$ entails absence of biaxial order [24].

Various specific parametrizations have been proposed and studied for V in Eq. (6): one of them is based on an approximate mapping from a hard-parallelepiped model [15]; another, more often studied one [16,18–22,24–28,36], is $\lambda=\gamma^2$; this can also be obtained by starting from a dispersion model *à la* London–de Boer–Heller approximation [37,38] and isotropically averaging over the orientation of the intermolecular vector (see, e.g., Refs. [16,20]); the fully anisotropic biaxial mesogenic dispersion model, also involving inner products of the molecular unit vectors $\{\boldsymbol{e},\boldsymbol{e}_\perp,\boldsymbol{m}\}$ and $\{\boldsymbol{e}',\boldsymbol{e}'_\perp,\boldsymbol{m}'\}$ with the intermolecular unit vector has been studied as well, both for three- and two-dimensional lattices [36,39].

The development of Ref. [23] started with the parametrization in Eq. (1) and it explored the existence and (mechanical) stability of a biaxial ground state. It then went on to study the simplified case $\gamma=0$. The stability analysis was performed by considering the variation δV of V for nearly parallel molecules

$$\delta V = \frac{U_0}{2}\alpha^2\{4\lambda w_m^2 + (1-2\gamma+\lambda)w_e^2 + (1+2\gamma+\lambda)w_\perp^2\} + O(\alpha^2), \quad (9)$$

where α is the angle of rotation that changes the relative orientation of two interacting molecules around the axis $\boldsymbol{w}\in\mathbb{S}^2$ represented by

$$\boldsymbol{w} = w_e\boldsymbol{e} + w_\perp\boldsymbol{e}_\perp + w_m\boldsymbol{m}. \quad (10)$$

The stability requirement that $\delta V>0$ is equivalent to the inequalities $\lambda>0$ and $2|\gamma|<1+\lambda$; moreover, the condition that the ground state be calamitic, that is, with the $\boldsymbol{m}$ axis harder to be disoriented than the other two, entails $2|\gamma|<1-3\lambda$. If we set $\gamma=0$, this condition restricts λ to the interval $0<\lambda<\frac{1}{3}$. When $\gamma=0$, the quadratic form (9) has two degenerate eigenvalues whose eigenspace is the plane spanned by $\{\boldsymbol{e},\boldsymbol{e}_\perp\}$; for $\lambda>\frac{1}{3}$, the degenerate eigenvalues are smaller than the eigenvalue associated with $\boldsymbol{m}$, and so, for $\lambda>\frac{1}{3}$, the planes orthogonal to $\boldsymbol{m}$ and $\boldsymbol{m}'$ are harder to disorient than all others, and this in turn promotes alignment between $\boldsymbol{m}$ and $\boldsymbol{m}'$. Thus, when $\gamma=0$, for either $0\leqslant\lambda\leqslant\frac{1}{3}$ and $\lambda\geqslant\frac{1}{3}$, the interaction potential in Eq. (5) promotes molecular alignment, albeit with apparently different mechanisms. This observation has motivated our extension of the analysis in Ref. [23] to the case $\lambda>\frac{1}{3}$.

The simplified model with $\gamma=0$ reveals a special symmetry property: the potential is invariant under $\pi/2$ rotations about $\boldsymbol{m}$ and $\boldsymbol{m}'$ in the individual molecular frames. More precisely, consider the rotation

$$\mathbf{R} = \mathbf{I} + \mathbf{W} + \mathbf{W}^2, \tag{11}$$

where $\mathbf{W}$ is the skew-symmetric tensor associated with $\boldsymbol{m}$

$$\mathbf{W} = \boldsymbol{e} \otimes \boldsymbol{e}_\perp - \boldsymbol{e}_\perp \otimes \boldsymbol{e}. \tag{12}$$

Imagine now the same rotation, but acting on the primed molecule. In the intrinsic frame of the molecule, it is represented by

$$\mathbf{R}' = \mathbf{I} + \mathbf{W}' + \mathbf{W}'^2, \tag{13}$$

where

$$\mathbf{W}' = \boldsymbol{e}' \otimes \boldsymbol{e}'_\perp - \boldsymbol{e}'_\perp \otimes \boldsymbol{e}'. \tag{14}$$

The transformed molecular tensors are then

$$\mathbf{q}^* = \mathbf{R}\mathbf{q}\mathbf{R}^T = \mathbf{q}, \quad \mathbf{b}^* = \mathbf{R}\mathbf{b}\mathbf{R}^T = -\mathbf{b}, \tag{15}$$

$$\mathbf{q}'^* = \mathbf{R}'\mathbf{q}'\mathbf{R}'^T = \mathbf{q}', \quad \mathbf{b}'^* = \mathbf{R}'\mathbf{b}'\mathbf{R}'^T = -\mathbf{b}', \tag{16}$$

and it can be shown from Eq. (1) that

$$V(\mathbf{q}^*, \mathbf{b}^*, \mathbf{q}'^*, \mathbf{b}'^*) = V(\mathbf{q}, \mathbf{b}, \mathbf{q}', \mathbf{b}') \Leftrightarrow \gamma = 0. \tag{17}$$

Thus, the special model $\gamma=0$ can be characterized by this symmetry, which is often referred to as the D_{4h} symmetry. Moreover, this special model possesses further symmetries. It can be shown that, for $\lambda=\frac{1}{3}$, V is also invariant under $\pi/2$ rotations about $\boldsymbol{e}$ and $\boldsymbol{e}'$, and under $\pi/2$ rotations about $\boldsymbol{e}_\perp$ and $\boldsymbol{e}'_\perp$ in the individual molecular frames. These rotations are associated with the following skew-symmetric tensors:

$$\mathbf{W}_e = \boldsymbol{e}_\perp \otimes \boldsymbol{m} - \boldsymbol{m} \otimes \boldsymbol{e}_\perp, \quad \mathbf{W}'_e = \boldsymbol{e}'_\perp \otimes \boldsymbol{m}' - \boldsymbol{m}' \otimes \boldsymbol{e}'_\perp,$$

$$\mathbf{W}_\perp = \boldsymbol{m} \otimes \boldsymbol{e} - \boldsymbol{e} \otimes \boldsymbol{m}, \quad \mathbf{W}'_\perp = \boldsymbol{m}' \otimes \boldsymbol{e}' - \boldsymbol{e}' \otimes \boldsymbol{m}'. \tag{18}$$

The corresponding invariant pair potential takes the special form

$$V = -\frac{2}{3} U_0 \{(\boldsymbol{m}\cdot\boldsymbol{m}')^2 + (\boldsymbol{e}\cdot\boldsymbol{e}')^2 + (\boldsymbol{e}_\perp\cdot\boldsymbol{e}'_\perp)^2 - 1\}. \tag{19}$$

In the following sections we shall explore the consequences of these pairwise potential symmetries over the order parameters' manifold and over the equilibrium phases.

III. MEAN-FIELD TREATMENT

In this section, starting from the potential in Eq. (4) with $\xi=1$ and $\gamma=0$, we build our mean-field theory. We consider an ensemble of biaxial molecules, within which the orientation of each molecule is specified with respect to a fixed reference frame $\{\boldsymbol{e}_x, \boldsymbol{e}_y, \boldsymbol{e}_z\}$ via a triplet of Euler angles $\omega=(\varphi, \vartheta, \psi)$ such that [23]

$$\begin{aligned}\boldsymbol{e} &= (\cos\psi\cos\varphi\cos\vartheta - \sin\psi\sin\varphi)\boldsymbol{e}_x \\ &\quad + (\cos\psi\sin\varphi\cos\vartheta + \sin\psi\cos\varphi)\boldsymbol{e}_y - \cos\psi\sin\vartheta\boldsymbol{e}_z,\end{aligned}$$

$$\begin{aligned}\boldsymbol{e}_\perp &= -(\sin\psi\cos\varphi\cos\vartheta + \cos\psi\sin\varphi)\boldsymbol{e}_x \\ &\quad - (\sin\psi\sin\varphi\cos\vartheta - \cos\psi\cos\varphi)\boldsymbol{e}_y + \sin\psi\sin\vartheta\boldsymbol{e}_z,\end{aligned}$$

$$\boldsymbol{m} = \cos\varphi\sin\vartheta\boldsymbol{e}_x + \sin\varphi\sin\vartheta\boldsymbol{e}_y + \cos\vartheta\boldsymbol{e}_z. \tag{20}$$

The liquid crystal phase is described by the order parameters introduced by Straley [15], which also represent the two independent second-rank order tensors [23] defined as ensemble averages of $\mathbf{q}$ and $\mathbf{b}$

$$\mathbf{Q} := \langle\mathbf{q}\rangle = S\left(\boldsymbol{e}_z \otimes \boldsymbol{e}_z - \frac{1}{3}\mathbf{I}\right) + T(\boldsymbol{e}_x \otimes \boldsymbol{e}_x - \boldsymbol{e}_y \otimes \boldsymbol{e}_y), \tag{21}$$

$$\mathbf{B} := \langle\mathbf{b}\rangle = S'\left(\boldsymbol{e}_z \otimes \boldsymbol{e}_z - \frac{1}{3}\mathbf{I}\right) + T'(\boldsymbol{e}_x \otimes \boldsymbol{e}_x - \boldsymbol{e}_y \otimes \boldsymbol{e}_y). \tag{22}$$

Alternatively, the order parameters (S, T, S', T') can be given as ensemble averages of the symmetry-adapted functions $s_k(\varphi, \vartheta, \psi)$

$$S = \langle s_1(\omega)\rangle, \quad T = \sqrt{\frac{2}{3}}\langle s_2(\omega)\rangle,$$

$$S' = \sqrt{6}\langle s_3(\omega)\rangle, \quad T' = 2\langle s_4(\omega)\rangle. \tag{23}$$

In this approximation, the pair potential is replaced by the pseudopotential (see, e.g., Refs. [16,17] and Refs. [26,27,29,31])

$$\Omega(\varphi, \vartheta, \psi) = -U_0\Psi, \tag{24}$$

where

$$\Psi = \sum_{jk=1}^{4} d_{jk}\langle s_j\rangle s_k = \mathbf{q}\cdot\mathbf{Q} + \lambda\mathbf{b}\cdot\mathbf{B}, \tag{25}$$

and the matrix D, with entries d_{jk}, is diagonal

$$[D] = \begin{pmatrix} \frac{2}{3} & 0 & 0 & 0 \\ 0 & \frac{4}{3} & 0 & 0 \\ 0 & 0 & 4\lambda & 0 \\ 0 & 0 & 0 & 8\lambda \end{pmatrix}. \tag{26}$$

The Boltzmann distribution function then reads as

$$f := \frac{1}{Z}\exp(\beta\Psi), \quad Z := \int_{\mathbb{T}} \exp(\beta\Psi)d\omega, \tag{27}$$

where $\beta := U_0/k_B t$, k_B is the Boltzmann constant, t is the absolute temperature, and Z is the partition function, in whose definition $\mathbb{T}$ denotes a toroidal manifold parametrized by the Euler angles $(\varphi, \vartheta, \psi)$ and $d\omega := \sin\vartheta d\vartheta d\varphi d\psi$ is the area measure on it. Accordingly, the mean-field free energy is

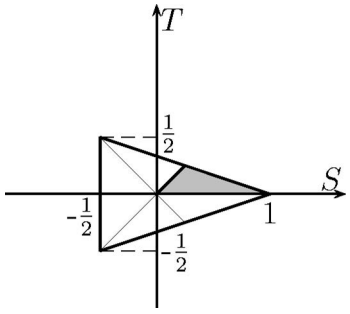

FIG. 1. (S,T)-plane projection of the state manifold $\mathcal{M}$.

$$\mathcal{F}(S,T,S',T';\beta,\lambda) = U_0\left\{\frac{1}{3}S^2+T^2+\frac{1}{3}\lambda S'^2+\lambda T'^2-\frac{1}{\beta}\ln\left(\frac{Z}{8\pi^2}\right)\right\} = U_0\left\{\frac{1}{2}\sum_{jk=1}^{4} d_{jk}\langle s_j\rangle\langle s_k\rangle-\frac{1}{\beta}\ln\left(\frac{Z}{8\pi^2}\right)\right\}. \quad (28)$$

As a consequence, four consistency conditions arise for the order parameters (S,T,S',T'):

$$S=\frac{1}{Z}\int_{\mathrm{T}} s_1\exp(\beta\Psi)d\omega, \quad (29)$$

$$T=\sqrt{\frac{2}{3}}\frac{1}{Z}\int_{\mathrm{T}} s_2\exp(\beta\Psi)d\omega, \quad (30)$$

$$S'=\frac{\sqrt{6}}{Z}\int_{\mathrm{T}} s_3\exp(\beta\Psi)d\omega, \quad (31)$$

$$T'=\frac{2}{Z}\int_{\mathrm{T}} s_4\exp(\beta\Psi)d\omega, \quad (32)$$

which also express the stationarity conditions for the free energy $\mathcal{F}$.

It follows from Eqs. (29)–(32) and the definitions in Eq. (8) that the order parameters are subject to the following bounds:

$$-\frac{1}{2}\leqslant S\leqslant 1,\quad -\frac{1}{3}(1-S)\leqslant T\leqslant\frac{1}{3}(1-S),$$

$$-(1-S)\leqslant S'\leqslant(1-S),\quad -1\leqslant T'\leqslant 1. \quad (33)$$

A rather telling geometric interpretation can be given for these bounds: the state manifold $\mathcal{M}$ can be represented as the Cartesian product $\mathcal{W}\times[-1,1]$, where $\mathcal{W}$ is the wedge in the (S,T,S') space defined by inequalities (33). Figure 1 shows the triangular base of $\mathcal{W}$ in the (S,T) plane. The vertices of this triangle represent the fully positive-ordered uniaxial states along the axis of the reference frame; the medians correspond to partially negative-ordered uniaxial states, with the isotropic state in their common intersection; any other point in the triangle represents a phase biaxial state, in the sense explained in Ref. [23]. Of course, each vertex represents the same uniaxial state, oriented along one of the three reference axes.

This equivalence property is indeed more general, as it applies to all inner points of the triangle: all points conjugated relative to one and the same median represent the same state with a different orientation. As a consequence, the states represented by the shaded region in Fig. 1 cover all possible (S,T) states of the system. Clearly, the symmetry transformations thus illustrated in the (S,T) plane act accordingly in the (S',T') plane; formally, they are described by the mappings

$$(S,T,S',T')\mapsto(S,-T,S',-T'),$$

$$(S,T,S',T')\mapsto\left(\frac{\pm 3T-S}{2},\frac{T\pm S}{2},\frac{\pm 3T'-S'}{2},\frac{T'\pm S'}{2}\right). \quad (34)$$

These transformations and all their combinations leave $\mathcal{F}$ invariant. Moreover, the D_{4h} symmetry of the pair-potential V in the special case $\xi=1$, $\gamma=0$ implies a further symmetry for the order parameters: since the transformation $(\mathbf{q},\mathbf{b})\mapsto(\mathbf{q},-\mathbf{b})$ leaves V unchanged, so does the transformation $(\mathbf{Q},\mathbf{B})\mapsto(\mathbf{Q},-\mathbf{B})$ with $\mathcal{F}$, as the distribution function f inherits the invariance properties of the pair potential. In terms of the order parameters (S,T,S',T'), this transformation becomes

$$(S,T,S',T')\mapsto(S,T,-S',-T'), \quad (35)$$

and, by composition with the first of (34), it induces a further symmetry transformation

$$(S,T,S',T')\mapsto(S,-T,-S',T'). \quad (36)$$

Like (34), both (35) and (36) also leave $\mathcal{F}$ invariant. All these symmetry transformations for the order parameters have profound consequences on the bifurcation analysis of the mean-field theory, which we present in the following section.

IV. BIFURCATION ANALYSIS

By performing a bifurcation analysis of the compatibility equations (29)–(32), we explore the mean-field model for all values of the parameter $\lambda\geqslant\frac{1}{3}$, beyond the bound considered in Ref. [23] and in Ref. [31]. These equations transform equivariantly with respect to the symmetry transformations (34)–(36), which realize a $\mathbb{Z}_2$-symmetry set of operators. In particular, these symmetry transformations are linear functions acting on the state vector $p=(S,T,S',T')^T$ in $\mathcal{M}\subset\mathbb{R}^4$ and are represented by the following four involution operators:

$$[O_{1,2}] = \begin{pmatrix} -\frac{1}{2} & \pm\frac{3}{2} & 0 & 0 \\ \pm\frac{1}{2} & \frac{1}{2} & 0 & 0 \\ 0 & 0 & -\frac{1}{2} & \pm\frac{3}{2} \\ 0 & 0 & \pm\frac{1}{2} & \frac{1}{2} \end{pmatrix},$$

$$[O_3] = \begin{pmatrix} 1 & 0 & 0 & 0 \\ 0 & -1 & 0 & 0 \\ 0 & 0 & 1 & 0 \\ 0 & 0 & 0 & -1 \end{pmatrix}, \tag{37}$$

$$[O_4] = \begin{pmatrix} 1 & 0 & 0 & 0 \\ 0 & -1 & 0 & 0 \\ 0 & 0 & -1 & 0 \\ 0 & 0 & 0 & 1 \end{pmatrix},$$

such that $O_i = O_i^{-1}$ for $i = 1,2,3,4$. We write the compatibility equations (29)–(32) in the form

$$p = g(p,\beta,\lambda), \tag{38}$$

where g is the $\mathbb{R}^4$-valued function representing the right-hand sides of these equations. The $\mathbb{Z}_2$ equivariance of these equations under O_i means that

$$g(O_i p,\beta,\lambda) = O_i g(p,\beta,\lambda)\ \forall\ (\beta,\lambda), \quad i = 1,2,3,4. \tag{39}$$

Since each operator O_i is an involution, it possesses eigenvalues $+1$ and -1, and so it induces a decomposition of $\mathbb{R}^4$, the ambient of the state manifold $\mathcal{M}$, into a symmetric submanifold where

$$O_i p = p, \tag{40}$$

and an antisymmetric submanifold where

$$O_i p = -p. \tag{41}$$

As explained above (see Fig. 1), the operators O_1, O_2, and O_3 realize only a reparametrization of the states, while the additional symmetry O_4 combined with O_3 makes the states $(S,0,0,0)$ special solutions, since they represent the common symmetric states with respect to both these operators and to their product O_3O_4, which is a $\mathbb{Z}_2$-operator as well. Actually such states represent the classical Maier-Saupe model [40], which is recovered in our setting for $\lambda = 0$. Thus, for $\gamma = 0$, the Maier-Saupe solution is a solution for all λ. This solution satisfies the following equation:

$$S = \frac{\int_0^\pi s_1(\vartheta)\exp\left[\frac{2}{3}\beta S s_1(\vartheta)\right]\sin\vartheta d\vartheta}{\int_0^\pi \exp\left[\frac{2}{3}\beta S s_1(\vartheta)\right]\sin\vartheta d\vartheta}, \tag{42}$$

which includes the isotropic state (0,0,0,0) as a special solution. The isotropic phase is locally unstable for $\beta > \beta_* = \frac{15}{2}$.

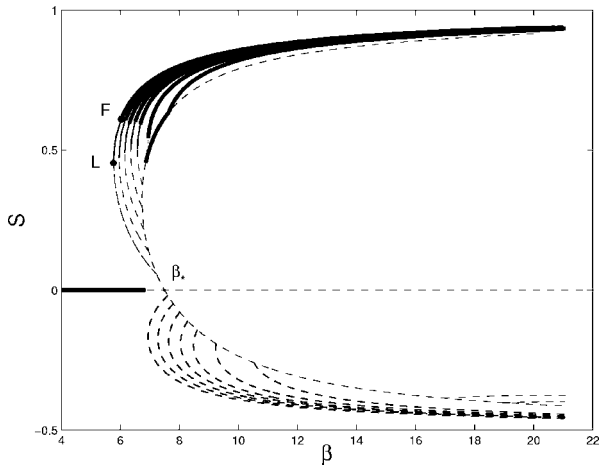

FIG. 2. Order parameter S versus β for different values of λ in the range $[0,\frac{1}{3}]$, contrasted with the Maier-Saupe solution $S_0(\beta)$, whence all graphs start. Here, $\beta_* = \frac{15}{2}$. As λ increases, these branches progressively retract away from the Maier-Saupe curve. The stable solutions with the least free energy correspond to the thick solid lines on the branches bifurcating from the positive side of the curve $S_0(\beta)$: they are associated with the order parameter T' depicted in Fig. 3. The dashed branches bifurcating from the negative side of the curve $S_0(\beta)$ are unstable solutions associated with the order parameter S'. The point F represents the transition point, while the point L represents the limit of stability, marked here only on one curve, to avoid clutter.

We denote by $S_0(\beta)$ the nonzero solution of (42), which exists in the range $\beta > \beta^* \approx 6.73$.

When $\lambda = 0$, it has long been known that for $\beta > \beta_c \approx 6.81$, a first-order transition occurs from the isotropic phase, which establishes a uniaxial state with $S = S_0(\beta)$. When $\lambda > 0$, further equilibrium states can be established by *breaking* the symmetry of the uniaxial state. In the formal language introduced in Refs. [41,42], the $\mathbb{Z}_2$ operators O_3 and O_4 are responsible for such a breaking, so that a branch of equilibrium solutions bifurcates in each relevant antisymmetric submanifold of $\mathcal{M}$. The symmetry-breaking bifurcation lines in the (β,λ) plane can be expressed in the analytical forms

$$\lambda_{S'}(\beta) = \frac{4}{2[1 - S_0(\beta)]\beta - 3}, \tag{43}$$

and

$$\lambda_{T'}(\beta) = \frac{24}{2[5 + 7S_0(\beta)]\beta - 3}, \tag{44}$$

corresponding to the solutions of the extended system associated with the symmetry decomposition induced by the operators O_4 and O_3, respectively (the interested reader is referred to Chap. VI of Ref. [41] and Chap. 8 of Ref. [43] for the technical details of this terminology).

Numerical computations show two bifurcation branches emanating from the Maier-Saupe curve when λ is not too large; upon further increasing λ, the two bifurcating branches are completely wrapped around it (Fig. 2). For small values

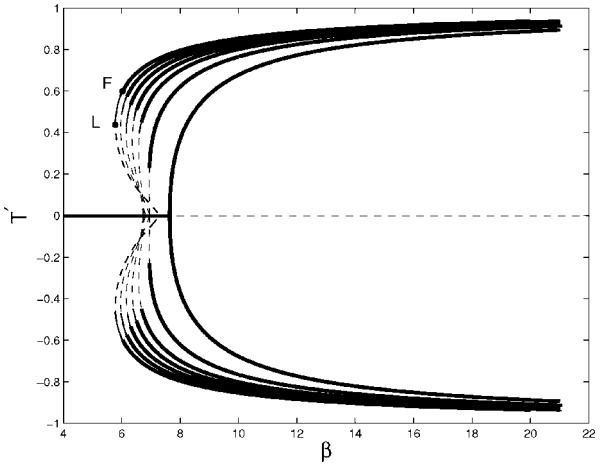

FIG. 3. Order parameter T' versus β for different values of λ in the range $[0,\frac{1}{3}]$. These curves correspond to the dominant solutions bifurcating from the positive side of the curve $S_0(\beta)$ in Fig. 2. F and L denote the corresponding transition point and limit of stability.

of λ, one of these branches breaks the symmetry in T', it keeps $T=S'=0$ (Figs. 2 and 3), and requires λ to exceed $\lambda_{T'}$ in (44); the other branch breaks the symmetry in S', it keeps $T=T'=0$ (Figs. 2 and 4), and requires λ to exceed $\lambda_{S'}$ in (43). The solution with $T'\neq 0$ has $S>0$ and represents a biaxial phase. The solution with $S'\neq 0$ has $S<0$ and represents a uniaxial phase since $T=T'=0$. This uniaxial phase is always locally unstable, and so no bifurcation occurs when $\lambda=\lambda_{S'}(\beta)$. The biaxial phase with $T'\neq 0$ is locally stable, at least for small values of λ, and so a bifurcation with exchange of stability occurs when $\lambda=\lambda_{T'}(\beta)$. A second-order phase transition then establishes a biaxial macroscopic ordering. First-order phase transitions are also possible when λ is increased [23].

For an assigned value of λ, a first-order transition occurs wherever the free energy of the condensed phase is equal to the free energy of the isotropic phase, which is zero, so that the compatibility equations (29)–(32) are solved together with the equation

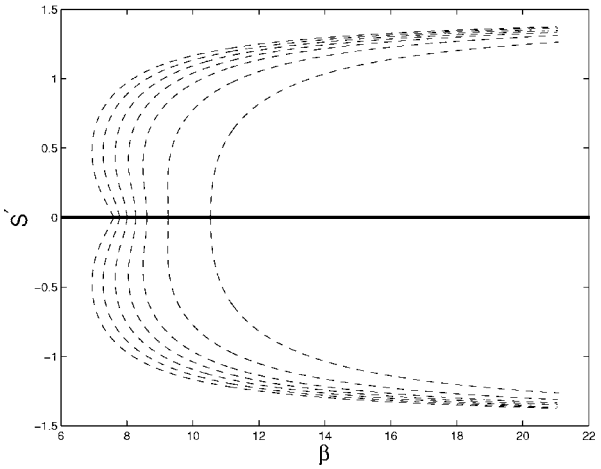

FIG. 4. Order parameter S' versus β for different values of λ in the range $[0,\frac{1}{3}]$. These curves correspond to the unstable solutions bifurcating from the negative side of the curve $S_0(\beta)$ in Fig. 2.

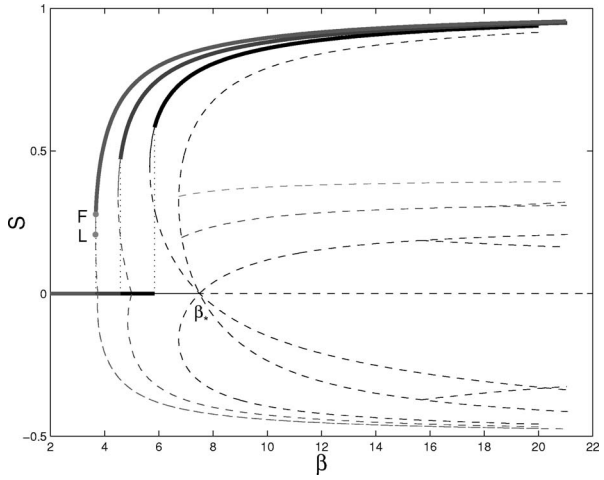

FIG. 5. Order parameter S versus β for $\lambda=\frac{1}{3},\frac{1}{2},\frac{2}{3}$. Two branches bifurcate from the isotropic state: the one with $S<0$ is locally unstable (dashed lines), while the one with $S>0$ becomes stable beyond the limit of stability L (thin solid lines). For $\lambda=\frac{1}{3}$, the two branches bifurcate at $\beta_*=\frac{15}{2}$; for $\lambda=\frac{1}{2}$ and $\lambda=\frac{2}{3}$, they bifurcate at $\beta=5$ and $\beta=\frac{15}{4}$, respectively. F marks the point at which the first-order transition takes place (and solid lines thicken). All other secondary bifurcating branches are unstable.

$$\mathcal{F}(S,T,S',T';\beta,\lambda)=0. \tag{45}$$

A first-order transition line is a collection of all solutions of this extended system.

In Figs. 2–4, thick solid lines represent phases with the least free energy, thin solid lines represent locally stable phases, and dashed lines represent locally unstable phases. L

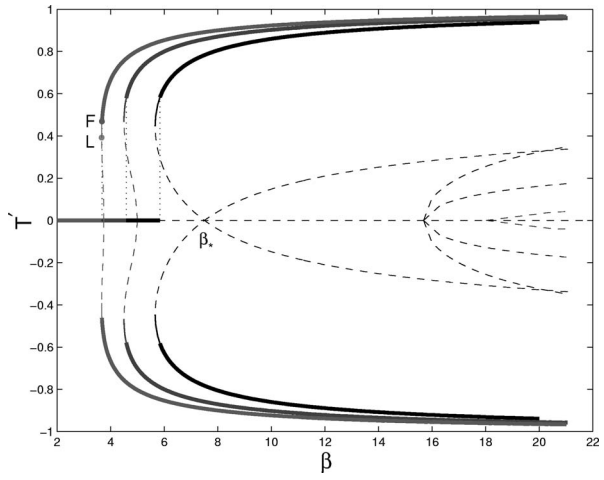

FIG. 6. Order parameter T' versus β for $\lambda=\frac{1}{3},\frac{1}{2},\frac{2}{3}$. Two symmetric branches bifurcate from the isotropic state: they are both associated with the positively ordered solutions in Fig. 5. All branches bifurcate backwards in β and are locally stable past the limit of stability L, while the first-order biaxial transition takes place at the point F. For $\lambda=\frac{1}{3}$, the tangent at the bifurcation point is oblique, whereas it is vertical for the other values of λ. For $\lambda=\frac{1}{3}$, the two branches bifurcate at $\beta_*=\frac{15}{2}$; for $\lambda=\frac{1}{2}$ and $\lambda=\frac{2}{3}$, they bifurcate at $\beta=5$ and $\beta=\frac{15}{4}$, respectively.

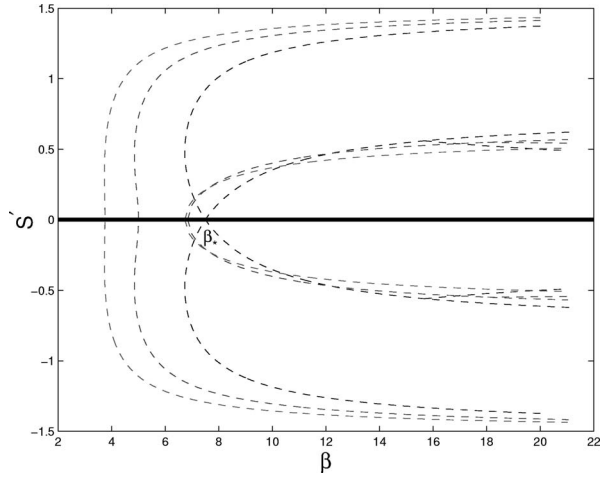

FIG. 7. Order parameter S' versus β for $\lambda=\frac{1}{3},\frac{1}{2},\frac{2}{3}$. Symmetric unstable branches emanate from the isotropic state, associated with the negatively ordered solution in Fig. 5.

denotes a limit point (limit of stability) where stable and unstable branches meet. F denotes a first-order transition point, where an ordered phase, either uniaxial or biaxial, attains less free energy than the isotropic phase.

It is shown in Fig. 3 how upon increasing λ in the range $[0,\frac{1}{3}]$, the biaxial branch starts bifurcating backwards, losing its stability in the vicinity of the bifurcation point. This is the manifestation of a tricritical point, where the uniaxial-to-biaxial transition changes from second- to first order [23]. Another tricritical point was recently predicted for this mean-field model along the isotropic-to-biaxial transition, which is expected to be first order for $\lambda<\frac{17}{21}$ and second order for $\lambda>\frac{17}{21}$ [32]. This prediction is now further explored within the present bifurcation analysis.

The symmetry-breaking bifurcation line associated with the operator O_3O_4 at the isotropic solution is

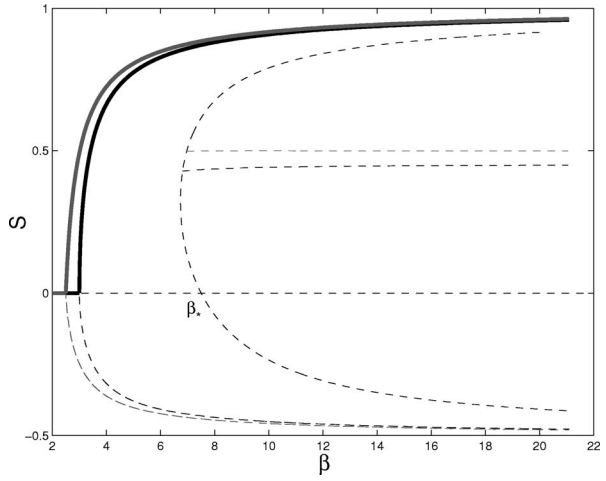

FIG. 8. Order parameter S versus β for $\lambda=\frac{5}{6},1$. Two branches bifurcate from $S=0$: one positive and stable and the other negative and unstable. A second-order phase transition occurs: here, both the limit of stability and the transition point coalesce into the bifurcation point. For $\lambda=\frac{5}{6}$, the bifurcation occurs at $\beta=3$, while for $\lambda=1$, it occurs at $\beta=\frac{5}{2}$. Here, $\beta_*=\frac{15}{2}$.

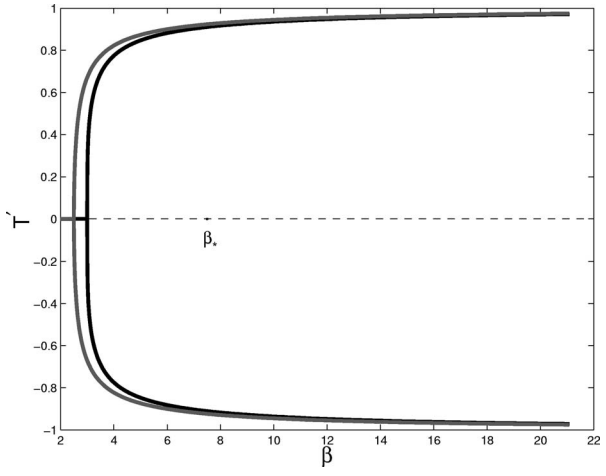

FIG. 9. Order parameter T' versus β for $\lambda=\frac{5}{6},1$. Two symmetric stable branches bifurcate at the same value of β as S in Fig. 8: they both correspond to the positively ordered state $S>0$.

$$\lambda_{S',T'}(\beta)=\frac{5}{2\beta}. \tag{46}$$

For $\lambda>\frac{1}{3}$, the critical value of β delivered by Eq. (46) is smaller than $\beta_*=\frac{15}{2}$, and the ordered solutions bifurcate from the isotropic state away from the classical Maier-Saupe solution. The bifurcation scenario evolves as depicted in Figs. 5–7, which represent the variety of equilibrium solutions for S, T', and S'. Both branches in T' and S' bifurcate from the same point in Eq. (46). The graphs for T are not reproduced here because T is negligible at all primary bifurcations. As shown in Fig. 5, two branches emanate from the isotropic state at $\beta=5/2\lambda$: the one with $S<0$ is always locally unstable, while the other becomes stable beyond the limit point. Two S' branches are also associated with the negatively ordered solutions: they are both unstable (see Fig. 7). Similarly, two symmetric T' branches are associated with the positively ordered solution: they both bifurcate backwards in β and are locally stable only past a limit point. A first-order transition

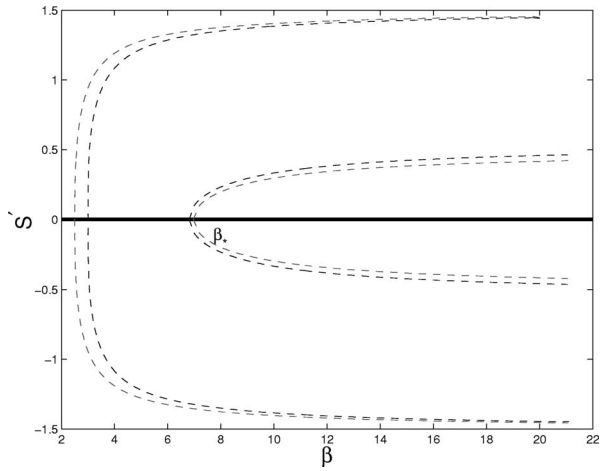

FIG. 10. Order parameter S' versus β for $\lambda=\frac{5}{6},1$. Two symmetric unstable branches emanate from $S'=0$, corresponding to the negatively ordered state $S<0$ in Fig. 8.

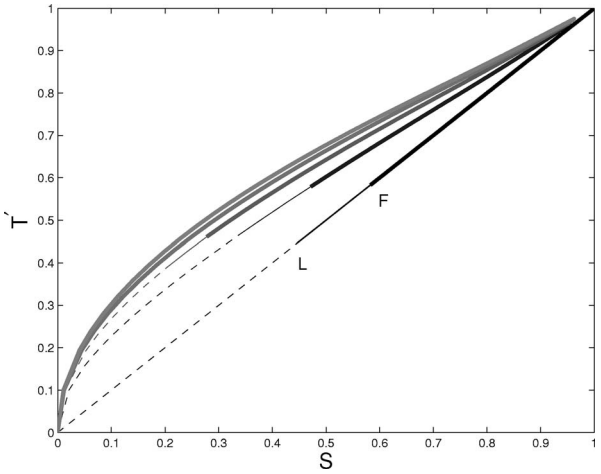

FIG. 11. Order parameter T' versus order parameter S for $\lambda=\frac{1}{3},\frac{1}{2},\frac{2}{3},\frac{5}{6},1$. For $\lambda=\frac{1}{3}$, the two order parameters are identical, as a result of the symmetry enjoyed there by the interaction potential V. Both the limit point L and the first-order transition point F are marked on the lines where they do not coincide with the bifurcation point.

occurs involving jumps of both S and T' from zero onto the stable bifurcated branches: correspondingly, the system undergoes a first-order isotropic-to-biaxial phase transition. For completeness, Figs. 5–7, also exhibit all secondary bifurcation branches we found with the continuation method employed here (the pseudo-arclength continuation [44]): they all emanate from solutions that are either unstable or with higher free energy.

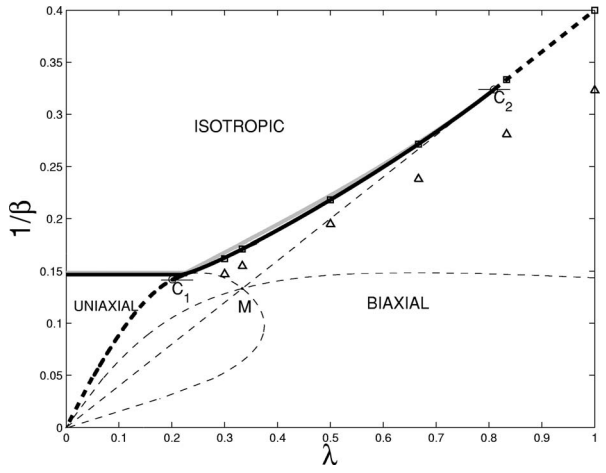

FIG. 12. Phase diagram (thick black lines) and stability diagram (gray lines) showing the reduced temperature $1/\beta$ versus the interaction parameter λ. Solid thick black lines mark all first-order phase transitions; the dashed thick black lines mark all second-order transitions. C_1 and C_2 are the two tricritical points, M is the common intersection of the symmetry-breaking lines in Eqs. (43), (44), and (46) (represented here as dashed thin lines, wherever differing from second-order transition lines). Triangles represent Monte Carlo (MC) results, and squares mark the corresponding mean-field predictions. The results obtained in Ref. [31] for $\lambda=\frac{3}{10}$ are displayed here together with the results obtained in this study for $\frac{1}{3},\frac{1}{2},\frac{2}{3},\frac{5}{6}$, and 1. (See also Tables I and II.)

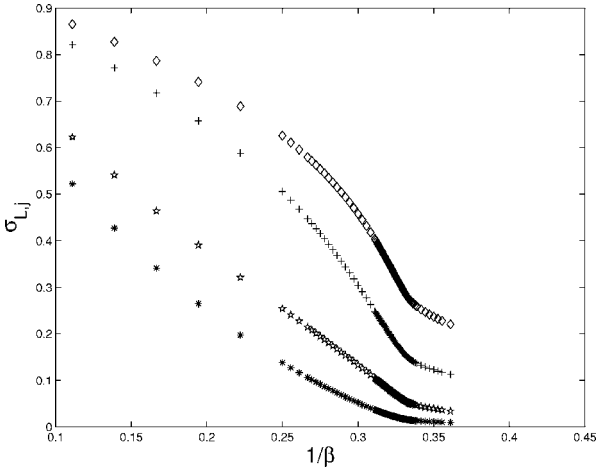

FIG. 13. Simulation results for short-range order parameter $\sigma_{L,j}$, obtained for $\lambda=1$ and with the largest sample size $l=30$. Discrete symbols have the following meanings: diamonds: $\sigma_{2,1}$; crosses: $\sigma_{2,3}$; stars: $\sigma_{4,1}$; asterisks: $\sigma_{4,3}$.

By continuing in λ the bifurcation analysis of the equilibrium equations, we found that the scenario illustrated by Figs. 5–7 stays qualitatively unchanged up to $\lambda=\frac{17}{21}$, thus showing the persistence of a direct isotropic-to-biaxial first-order transition.

Above the tricritical point at $\lambda=\frac{17}{21}$, the bifurcation scenario yet changes again. Figures 8–10 show the order parameters S, T', and S' at equilibrium. Two branches bifurcate from $S=0$ in Fig. 8, one positive and the other negative: the former is stable, while the latter is unstable. This bifurcation occurs for β below β_*, and the Maier-Saupe curve, still represented in Fig. 8, is completely overshadowed by the early primary bifurcations. Two symmetric S' branches are associated with the negatively ordered nematic phase, but they are both unstable, as is the parent S branch (see Fig. 8); thus, $S'=0$ for all stable equilibrium solutions. Correspondingly,

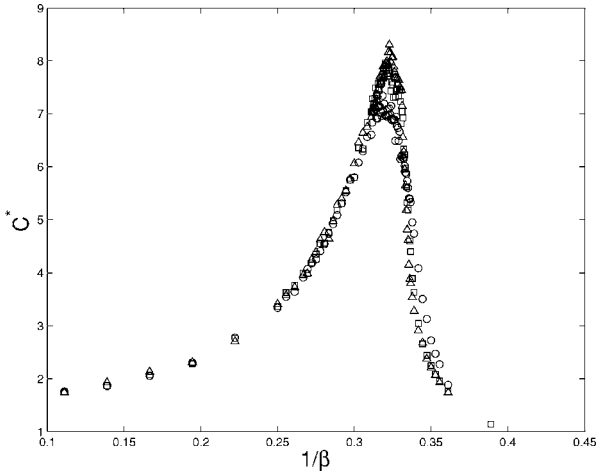

FIG. 14. Simulation results for the configurational heat capacity for $\lambda=1$; the discrete symbols correspond to different sample sizes, and have the following meanings: circles: $l=10$; squares: $l=20$; triangles: $l=30$. The associated statistical errors, not shown, range between 1% and 5%.

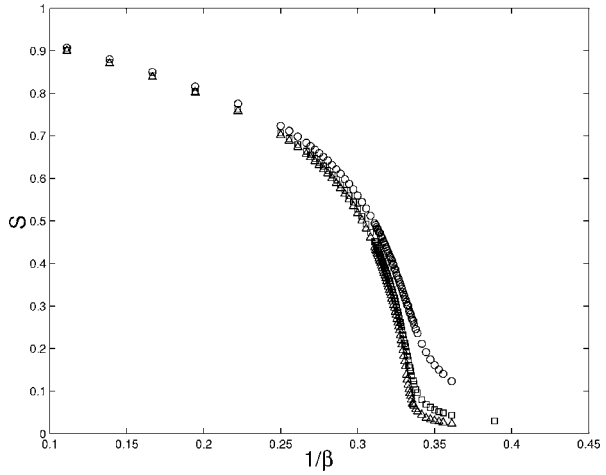

FIG. 15. Simulation results for the order parameters $S=\langle P_2\rangle = \langle s_1\rangle$ for $\lambda=1$, obtained with different sample sizes; same meaning of symbols as in Fig. 14.

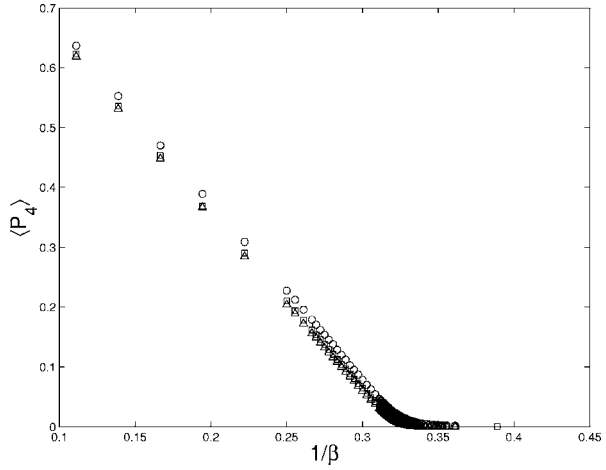

FIG. 17. Simulation results for the fourth-rank order parameter $\langle P_4\rangle$ for $\lambda=1$, obtained with different sample sizes; same meaning of symbols as in Fig. 14.

T' has two symmetric stable branches bifurcating at the same value of β as S. Thus, at $\lambda=\frac{17}{21}$ the isotropic-to-biaxial transition becomes second order and it remains so for all larger values of λ.

Still two order parameters, S and T', one pertaining to **Q** and the other to **B**, suffice to describe the whole variety of stable equilibrium phases. They are plotted together in Fig. 11 for $\lambda \geqslant \frac{1}{3}$. They become identical for $\lambda=\frac{1}{3}$, as a consequence of the special symmetry property enjoyed by V in Eq. (19).

A numerical continuation analysis [43] also allowed us to construct the phase diagram of this mean-field model, which is represented in Fig. 12 in the $(\lambda, 1/\beta)$ plane. In this figure, the symmetry-breaking bifurcation lines defined by Eqs. (43), (44), and (46) appear as dashed thin lines, all passing through the point M. The dashed thick line joining the origin and the tricritical point C_1 is the second-order uniaxial-to-biaxial transition line: it is part of the line represented by Eq. (44). The dashed thick line starting at C_2 is the second-order isotropic-to-biaxial transition line. The solid thick lines represent first-order transitions: those already found in Ref. [23] for $\lambda<\frac{1}{3}$ along with those found here for $\lambda>\frac{1}{3}$ between the two tricritical points. These lines were found by continuing in λ the solutions of the extended system consisting in the equilibrium equations and condition (45). For completeness, we also represent in Fig. 12 the limits of stability (gray thick line), obtained by continuing in λ the limit of stability on the biaxial branches $(S,0,0,T')$.

V. MONTE CARLO SIMULATIONS

In addition to the above "global" mean-field treatment, for assigned values of the potential parameter λ, one can numerically solve the consistency equations and minimize the mean-field free energy over a fine temperature grid, and thus calculate the temperature dependence for the resulting thermodynamic and structural properties. This procedure was used for a few selected values of λ, and the mean-field analy-

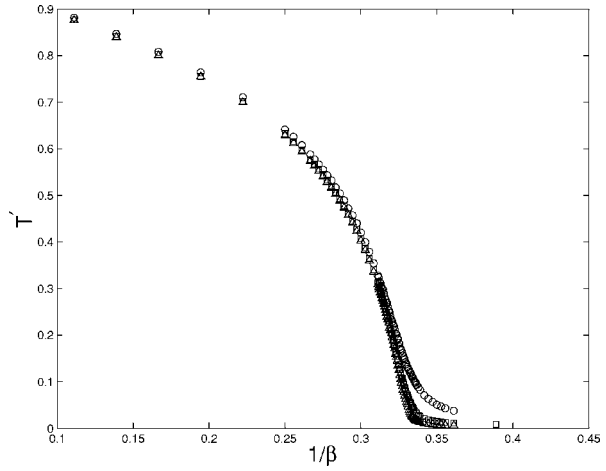

FIG. 16. Simulation results for the order parameter $T'=2\langle s_4\rangle$ for $\lambda=1$, obtained with different sample sizes; same meaning of symbols as in Fig. 14.

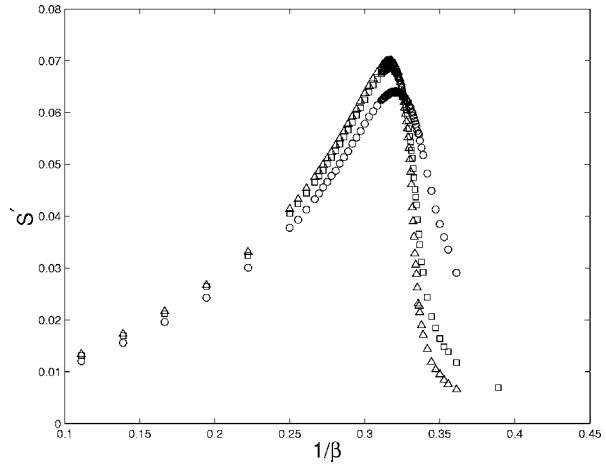

FIG. 18. Simulation results for the order parameter S' for $\lambda=1$, obtained with different sample sizes; same meaning of symbols as in Fig. 14.

TABLE I. Mean-field estimates for transitional properties, obtained with different values of λ (see Figs. 5, 6, 8, and 9). Blank lines correspond to second-order transitions, where order parameters and ΔU^*_{MF} are zero.

λ	$\left(\frac{1}{\beta}\right)_{MF,tr}$	ΔU^*_{MF}	S	T'	$\langle P_4 \rangle$
$\frac{3}{10}$	0.1618	0.2136	0.5967	0.5624	0.2395
$\frac{1}{3}$	0.1711	0.2275	0.5842	0.5842	0.2282
$\frac{1}{2}$	0.2180	0.2426	0.4726	0.5798	0.1443
$\frac{2}{3}$	0.2716	0.1816	0.2967	0.4780	0.0566
$\frac{5}{6}$	$\frac{1}{3}$				
1	$\frac{2}{5}$				

sis was supplemented by and compared with Monte Carlo simulation results, obtained for lattice models defined by the same λ values (the corresponding lattice models, for short). More precisely, we consider a three-dimensional simple-cubic lattice $\mathbb{Z}^3$ whose axes define the orthonormal basis $\{\boldsymbol{e}_x, \boldsymbol{e}_y, \boldsymbol{e}_z\}$. To each site μ, with coordinate vector $\boldsymbol{x}_\mu$, we associate a particle center of mass; the interaction potential V is restricted to nearest neighbors, involving molecules or sites labeled by μ and ν, respectively. Molecular orientations are specified via orthonormal triplets of three-component vectors, say $\{\boldsymbol{e}_\mu, \boldsymbol{e}_{\perp\mu}, \boldsymbol{m}_\mu\}$ for the molecule on the site μ and $\{\boldsymbol{e}_\nu, \boldsymbol{e}_{\perp\nu}, \boldsymbol{m}_\nu\}$ for the molecule sited in ν. The interaction potential is

$$V = \epsilon\{-P_2(\boldsymbol{m}_\mu \cdot \boldsymbol{m}_\nu) - \lambda[2P_2(\boldsymbol{e}_{\perp\mu} \cdot \boldsymbol{e}_{\perp\nu}) + 2P_2(\boldsymbol{e}_\mu \cdot \boldsymbol{e}_\nu) - P_2(\boldsymbol{m}_\mu \cdot \boldsymbol{m}_\nu)]\}, \tag{47}$$

where $\epsilon = \frac{2}{3}U_0$.

Allowing for a lattice situation, the mean-field formalism changes by appropriate numerical factors, as follows. Since each molecule interacts with its 6 nearest neighbors, the pseudopotential (24) is replaced by the following:

$$\tilde{\Omega} = 2\rho\Omega = -2\rho U_0 \Psi, \tag{48}$$

where $2\rho = 6$ is the coordination number for the simple-cubic lattice. Accordingly, the free energy becomes

$$\tilde{\mathcal{F}} = U_0 \left\{ \rho \sum_{jk=1}^{4} d_{jk} \langle s_j \rangle \langle s_k \rangle - \frac{1}{\beta} \ln\left(\frac{\tilde{Z}}{8\pi^2}\right) \right\}, \tag{49}$$

$$\tilde{Z} = \int_{\mathrm{T}} \exp(2\rho\beta\Psi) d\omega.$$

As a consequence, in actual simulations we used a temperature scale T^* which differs from $1/\beta$ by a factor of 9; this value results from the coordination number used for MC simulations, as well as from an energy scale of the microscopic potential differing from the one used in the preceding sections by a factor of $\frac{3}{2}$ (in turn, this was chosen so as to enforce a better compatibility with the Lebwohl-Lasher model); thus, the following mapping exists between the temperature scales:

$$T^* = \frac{k_B t}{\epsilon} = 9\left(\frac{1}{\beta}\right), \tag{50}$$

and simulation results were eventually converted to the $1/\beta$ scale for comparisons. The value $\lambda = \frac{3}{10}$ had been investigated in Ref. [31], and the following ones were investigated here: $\frac{1}{3}$, $\frac{1}{2}$, $\frac{2}{3}$, $\frac{5}{6}$, and 1. Let us recall that the above mean-field analysis predicts the existence of a direct isotropic-to-biaxial phase transition for $0.22 \lesssim \lambda \leqslant 1$ (see also Ref. [23]), being of first order up to $\lambda = \frac{17}{21} \approx 0.8095$, and of second order for higher λ. Simulations were carried on a periodically repeated cubic sample, consisting of $N = l^3$ particles, $l = 10, 20, 30$; calculations were run in cascade, in order of increasing temperature; each cycle (or sweep) consisted of $2N$ MC steps, including a sublattice sweep [50]; the finest temperature step used was $\Delta T^* = 0.0005$, in the transition region.

TABLE II. MC estimates for transitional properties, obtained with different values of λ, and based on the largest investigated sample size $l = 30$; simulation results for $\lambda = \frac{3}{10}$ have been taken from Ref. [31]. Blank lines correspond to second-order transitions, where order parameters and ΔU^* are zero.

λ	$\left(\frac{1}{\beta}\right)_{MC,tr}$	ΔU^*	S	T'	$\langle P_4 \rangle$
$\frac{3}{10}$	0.1471±0.0001	0.083±0.004	0.435±0.016	0.38±0.02	0.103±0.008
$\frac{1}{3}$	0.1548±0.0001	0.093±0.004	0.42±0.01	0.414±0.012	0.094±0.005
$\frac{1}{2}$	0.1948±0.0001	0.063±0.009	0.362±0.012	0.282±0.012	0.032±0.004
$\frac{2}{3}$	0.238±0.001				
$\frac{5}{6}$	0.281±0.001				
1	0.323±0.001				

Equilibration runs took between 25 000 and 200 000 cycles, and production runs took between 200 000 and 800 000; macrostep averages for evaluating statistical errors were taken over 1000 cycles. Calculated thermodynamic quantities include mean potential energy per site U^* (where the asterisk means scaling by ϵ) and configurational specific heat per particle C^* (where the asterisk means scaling by k_B).

The order parameters (S,T,S',T') were obtained by averaging the four symmetry-adapted functions s_k [45–49]

$$S=\langle s_1\rangle, \quad T=\sqrt{\frac{2}{3}}\langle s_2\rangle, \quad S'=\sqrt{6}\langle s_3\rangle, \quad T'=2\langle s_4\rangle; \tag{51}$$

they were calculated by analyzing a configuration every cycle, according to methodologies discussed in detail by other authors [26,30,47,48]; the four quantities $\langle s_k\rangle$ are all different from zero in a biaxial phase (although $\langle s_3\rangle$ and $\langle s_2\rangle$ may be rather small), while both $\langle s_2\rangle$ and $\langle s_4\rangle$ vanish in a uniaxial phase [47–49]. MC estimates of the fourth-rank order parameter $\langle P_4\rangle$ were determined as well [47–49,51,52].

We also evaluated the so-called short-range order parameters [47,48]

$$\sigma_{L,1}=\langle P_L(\boldsymbol{e}_\mu\cdot\boldsymbol{e}_\nu)\rangle, \quad \sigma_{L,2}=\langle P_L(\boldsymbol{e}_{\perp\mu}\cdot\boldsymbol{e}_{\perp\nu})\rangle, \tag{52}$$

$$\sigma_{L,3}=\langle P_L(\boldsymbol{m}_\mu\cdot\boldsymbol{m}_\nu)\rangle, \quad L=2,4,$$

measuring correlations between corresponding pairs of unit vectors $\boldsymbol{e}_\mu$, $\boldsymbol{e}_{\perp\mu}$, $\boldsymbol{m}_\mu$, and $\boldsymbol{e}_\nu$, $\boldsymbol{e}_{\perp\nu}$, $\boldsymbol{m}_\nu$, associated with nearest-neighbor molecules; the functional form of the interaction entails that the potential energy U^* is a linear combination of quantities $\sigma_{2,1}$, $\sigma_{2,2}$, and $\sigma_{2,3}$; here, the condition $\gamma=0$ entails $\sigma_{L,1}=\sigma_{L,2}$; moreover, when $\lambda=\frac{1}{3}$, $\sigma_{L,1}=\sigma_{L,2}=\sigma_{L,3}$.

Simulation results for the specific value $\lambda=1$ are reported and contrasted in the following figures. For $\lambda=\frac{1}{3},\frac{1}{2},\frac{2}{3}$, and $\frac{5}{6}$, MC results for several observables in the transition region are plotted in Ref. [53]. Transitional properties for all examined values of λ are collected and compared in Tables I and II; simulation results for $\lambda=\frac{3}{10},\frac{1}{3},\frac{1}{2}$ point to a first-order transition, whose character seems to weaken with increasing λ; on the other hand, simulation results for $\lambda=\frac{2}{3},\frac{5}{6},1$ suggest a second-order transition. Upon analyzing the simulation results for the largest sample as discussed in Refs. [54,55], we propose estimates for transitional properties as collected in Table II.

A. The case $\lambda=1$

The mean-field transition temperature for $\lambda=1$ was found to be $(1/\beta)_{MF,tr}=\frac{2}{5}$ from Eq. (46); here, potential energy U^*_{MF}

$$U^*_{MF}=-\frac{1}{2}\langle\tilde{\Omega}\rangle, \tag{53}$$

and order parameters vanish continuously; in this case, mean field predicts both $\langle s_3\rangle$ and $\langle s_2\rangle$ to be practically zero even in the biaxial phase, as found also in Ref. [23].

Simulation results for various properties are collected in Figs. 13–19. Observables such as $\sigma_{L,j}$ (and hence the potential energy $U^*\propto\sigma_{2,1}$) exhibit a gradual and monotonic change with temperature, and a very weak sample size dependency, so that only results obtained for the largest sample-size $l=30$ are plotted in Fig. 13; notice that in this case the term $P_2(\boldsymbol{m}_\mu\cdot\boldsymbol{m}_\nu)$ does not appear in the pair potential, yet $\sigma_{L,3}>0$, i.e., the parallelizing interaction between the two other pairs of unit vectors enforces correlations between the third pair.

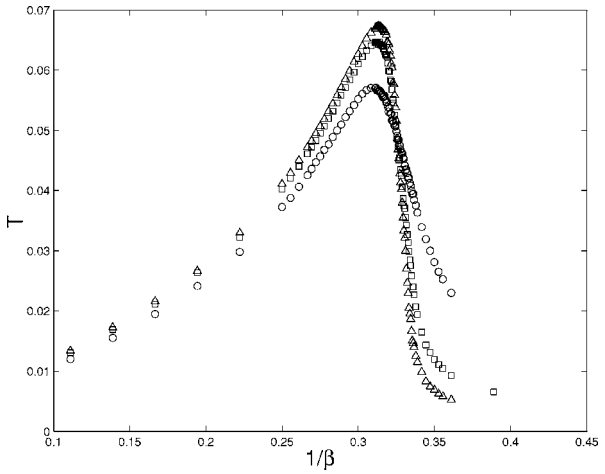

FIG. 19. Simulation results for the order parameter T for $\lambda=1$, obtained with different sample sizes; same meaning of symbols as in Fig. 14.

Results for C^* (Fig. 14) exhibit a more recognizable sample-size dependency, and show a peak at $1/\beta\approx0.322$.

Results for the order parameters are shown in Figs. 15–19; S, T', and $\langle P_4\rangle$ (Figs. 15–17) appear to decrease monotonically with temperature, whereas the other two order parameters T and S' (Figs. 18 and 19) increase up to a maximum at $1/\beta\approx0.317$ and then decrease; all the order parameters appear to evolve with temperature in a gradual and continuous way, and, for $1/\beta\gtrsim0.322$, all of them exhibit a pronounced decrease with increasing sample sizes.

Based on the above results, we propose a direct biaxial-to-isotropic continuous transition, and the value $(1/\beta)_{MC,tr}=0.323\pm0.001$ for the transition temperature; the estimated uncertainty is based on the temperature step used in the investigated range, and the ratio $(1/\beta)_{MC,tr}/(1/\beta)_{MF,tr}$ is 0.808.

VI. CONCLUSIONS

As far as models go, mean field shows that the simplified interaction with $\gamma=0$ in Eq. (1) is a biaxial mesogenic potential; upon increasing λ there is first a two-transition regime (biaxial-to-uniaxial and then uniaxial-to-isotropic), where the biaxial-to-uniaxial transition is first second order and then first order; for larger values of λ only the direct biaxial-to-isotropic transition survives, being first order, and then, for larger λ, second order.

Two tricritical points, C_1 and C_2, have been determined; in particular, C_2, the one predicted in Ref. [32], was confirmed by a bifurcation analysis, which showed how C_1 and C_2 are joined by a first-order transition line, very close to the limit of stability. MC simulations carried out on the corre-

sponding three-dimensional lattice models for $\lambda = \frac{1}{3}, \frac{1}{2}, \frac{2}{3}, \frac{5}{6}, 1$ qualitatively confirm this picture. More precisely, simulations suggest that already for $\lambda = \frac{2}{3}$ the direct isotropic-to-biaxial transition is second order, thus effectively reducing the span of the first-order transition expected between the points C_1 and C_2. This is perhaps the most striking difference between the model studied here, for which $\gamma = 0$, and the one for which $\gamma = \sqrt{\lambda}$, already explored in depth in the literature both within the mean-field approximation [18] and through computer simulation [27]: the direct isotropic-to-biaxial transition that for the latter model takes place at a singular Landau triple point happens for the former along a whole set of the interaction parameter λ, and—depending on λ—can be either first- or second order.

In a sense, the present potential models cry for extensions to the case $\gamma \neq 0$; work along these lines has been started, and will be reported in due course.

ACKNOWLEDGMENTS

We wish to thank Professor E. C. Gartland, Jr. (Kent State University, Ohio) and Dr. F. Bisi (University of Pavia, Italy) for helpful discussion and suggestions. The extensive Monte Carlo calculations were carried out, among other machines, on workstations, belonging to the Sezione di Pavia of Istituto Nazionale di Fisica Nucleare (INFN); allocations of computer time by the Computer Centre of Pavia University and CILEA (Consorzio Interuniversitario Lombardo per l' Elaborazione Automatica, Segrate -Milan), as well as by CINECA (Centro Interuniversitario Nord-Est di Calcolo Automatico, Casalecchio di Reno -Bologna), are gratefully acknowledged as well. Finally, we gratefully acknowledge financial support from the Italian Ministry for Higher Education (MIUR) through the PRIN Grant No. 2004024508.

[1] G. R. Luckhurst, Nature (London) **430**, 413 (2004).
[2] L. J. Yu and A. Saupe, Phys. Rev. Lett. **45**, 1000 (1980).
[3] S. M. Fan, I. D. Fletcher, B. Gündoğan, N. J. Heaton, G. Kothe, G. R. Luckhurst, and K. Praefcke, Chem. Phys. Lett. **204**, 517 (1993).
[4] G. R. Luckhurst, Thin Solid Films **393**, 40 (2001).
[5] K. Praefcke, Mol. Cryst. Liq. Cryst. Sci. Technol., Sect. A **364**, 15 (2001).
[6] K. Praefcke, Braz. J. Phys. **32**, 564 (2002).
[7] L. A. Madsen, T. J. Dingemans, M. Nakata, and E. T. Samulski, Phys. Rev. Lett. **92**, 145505 (2004).
[8] B. R. Acharya, A. Primak, and S. Kumar, Liq. Cryst. Today **13**, 1 (2004).
[9] B. R. Acharya, A. Primak, and S. Kumar, Phys. Rev. Lett. **92**, 145506 (2004).
[10] K. Severing and K. Saalwächter Phys. Rev. Lett. **92**, 125501 (2004).
[11] K. Merkel, A. Kocot, J. K. Vij, R. Korlacki, G. H. Mehl, and T. Meyer, Phys. Rev. Lett. **93**, 237801 (2004).
[12] M. J. Freiser, Phys. Rev. Lett. **24**, 1041 (1970).
[13] M. J. Freiser, Mol. Cryst. Liq. Cryst. **14**, 165 (1971).
[14] R. Alben, Phys. Rev. Lett. **30**, 778 (1973).
[15] J. P. Straley, Phys. Rev. A **10**, 1881 (1974).
[16] G. R. Luckhurst, C. Zannoni, P. L. Nordio, and U. Segre, Mol. Phys. **30**, 1345 (1975).
[17] R. L. Humphries, P. G. James, and G. R. Luckhurst, J. Chem. Soc., Faraday Trans. 2 **68**, 1031 (1972).
[18] N. Boccara, R. Mejdani, and L. De Seze, J. Phys. (Paris) **38**, 149 (1976).
[19] D. K. Remler and A. D. J. Haymet, J. Phys. Chem. **90**, 5426 (1986).
[20] B. Bergersen, P. Palffy-Muhoray, D. A. Dunmur, Liq. Cryst. **3**, 347 (1988).
[21] Zhang Zhi-Dong and Huang Xi-Min, Acta Phys. Sin. (Overseas Ed.) **6**, 671 (1997).
[22] M. Hosino and H. Nakano, Mol. Cryst. Liq. Cryst. Sci. Technol., Sect. A **348**, 207 (2000).
[23] A. M. Sonnet, E. G. Virga, and G. E. Durand, Phys. Rev. E **67**, 061701 (2003).
[24] G. R. Luckhurst and S. Romano, Mol. Phys. **40**, 129 (1980).
[25] C. D. Mukherjee and N. Chatterjee, Phys. Lett. A **189**, 86 (1994).
[26] F. Biscarini, C. Chiccoli, P. Pasini, F. Semeria, and C. Zannoni, Phys. Rev. Lett. **75**, 1803 (1995).
[27] C. Chiccoli, P. Pasini, F. Semeria, and C. Zannoni, Int. J. Mod. Phys. C **10**, 469 (1999).
[28] P. Pasini, C. Chiccoli, and C. Zannoni, *Advances in the Computer Simulations of Liquid Crystals*, edited by P. Pasini and C. Zannoni, NATO Science Series (Kluwer, Dordrecht, 2000), Vol. C545, Chap. 5.
[29] B. Mulder, Phys. Rev. A **39**, 360 (1989).
[30] M. P. Allen, Liq. Cryst. **8**, 499 (1990).
[31] S. Romano, Physica A **337**, 505 (2004).
[32] G. De Matteis and E. G. Virga, Phys. Rev. E **71**, 061703 (2005).
[33] D. M. Brink and G. R. Satchler, *Angular Momentum*, 2nd ed., (Oxford University Press, Oxford, UK, 1968).
[34] D. A. Varshalovich, A. N. Moskalev, and V. K. Khersonskii, *Quantum Theory of Angular Momentum* (World Scientific, Singapore, 1988).
[35] G. B. Arfken and H. J. Weber, *Mathematical Methods for Physicists*, 4th ed. (Academic Press, San Diego, 1995).
[36] S. Romano, Physica A **339**, 511 (2004).
[37] A. D. Buckingham, in *Intermolecular Forces*, edited by J. O. Hirschfelder (Wiley, London, 1967), Chap. 2 [Adv. Chem. Phys. **12**, 107 (1967)].
[38] C. G. Gray and K. E. Gubbins, *Theory of Molecular Fluids, Vol. 1: Fundamentals* (Oxford University Press, Oxford, UK, 1984).
[39] S. Romano, Physica A **339**, 491 (2004).
[40] W. Maier and A. Saupe, Z. Naturforsch. A **14a**, 882 (1959).
[41] M. Golubitsky and D. G. Schaeffer, *Singularities and Groups in Bifurcation Theory* (Springer-Verlag, Berlin, 1985), Vol. 1.
[42] M. Golubitsky, I. Stewart, and D. G. Schaeffer, *Singularities and Groups in Bifurcation Theory* (Springer-Verlag, Berlin, 1988), Vol. 2.

[43] Willy J. F. Govaerts, *Numerical Methods for Bifurcations of Dynamical Equilibria* (SIAM, Philadelphia, 2000).
[44] E. J. Doedel, R. C. Paffenroth, A. R. Champneys, T. F. Fairgrieve, Y. A. Kuznetsov, B. E. Oldeman, B. Sandstede, and X. Wang, Tech. Report, Concordia University, Montreal, Canada (2002).
[45] M. A. Bates and G. R. Luckhurst, Struct. Bonding (Berlin) **94**, 65 (1998).
[46] A. Ferrarini, P. L. Nordio, E. Spolaore, and G. R. Luckhurst, J. Chem. Soc., Faraday Trans. **91**, 3177 (1995).
[47] C. Zannoni, *The Molecular Physics of Liquid Crystals*, edited by G. R. Luckhurst and G. W. Gray (Academic Press, London, 1979), Chaps. 3 and 9.
[48] C. Zannoni, *Advances in the Computer Simulations of Liquid Crystals*, edited by P. Pasini and C. Zannoni, NATO Science Series, (Kluwer, Dordrecht, 2000), Vol. c545, Chap. 2.
[49] G. R. Luckhurst, *Physical Properties of Liquid Crystals: Nematics*, edited by D. A. Dunmur, A. Fukuda, and G. R. Luckhurst, (INSPEC, London, UK, 2001), Chap. 2.1.
[50] R. Hashim and S. Romano, Int. J. Mod. Phys. B **13**, 3879 (1999).
[51] U. Fabbri and C. Zannoni, Mol. Phys. **58**, 763 (1986).
[52] C. Chiccoli, P. Pasini, F. Biscarini, and C. Zannoni, Mol. Phys. **65**, 1505 (1988).
[53] See EPAPS Document No. E-PLEEE8-72-071510 for Additional simulation results. This document can be reached via a direct link in the online article's HTML reference section or via the EPAPS homepage (http://www.aip.org/pubservs/epaps.html).
[54] S. Romano, Int. J. Mod. Phys. B **16**, 2901 (2002).
[55] S. Romano, Physica A **324**, 606 (2003).